Synthesis and Structure of the Ruthenium(II) Complexes $[(\eta\text{-}C_5Me_5)Ru(NO)(bipy)]^{2+}$ and $[(\eta\text{-}C_5Me_5)Ru(NO)(dppz)]^{2+}$. DNA Cleavage by an Organometallic dppz Complex (bipy = 2,2′-Bipyridine; dppz = Dipyrido[3,2-*a*:2′,3′-*c*]phenazine)

Thomas K. Schoch, John L. Hubbard,* Christopher R. Zoch, Geun-Bae Yi, and Morten Sørlie

Department of Chemistry and Biochemistry, Utah State University, Logan, Utah 84322-0300

Received June 15, 1995[⊗]

The salts $[(\eta\text{-}C_5Me_5)Ru(NO)(bipy)][OTf]_2$ (**1**$[OTf]_2$) and $[(\eta\text{-}C_5Me_5)Ru(NO)(dppz)][OTf]_2$ (**2**$[OTf]_2$) are obtained from the treatment of $(\eta\text{-}C_5Me_5)Ru(NO)(OTf)_2$ with 2,2′-bipyridine (bipy) or dipyrido[3,2-*a*:2′,3′-*c*]phenazine (dppz) (OTf = OSO_2CF_3). X-ray data for **1**$[OTf]_2$: monoclinic space group $P2_1/c$, $a = 11.553$ (4) Å, $b = 16.517$ (5) Å, $c = 14.719$ (4) Å, $\beta = 94.01$ (2)°, $V = 2802$ (2) Å^3, $Z = 4$, R1 = 0.0698. X-ray data for **2**$[OTf]_2$: monoclinic space group $P2_1/c$, $a = 8.911$ (2) Å, $b = 30.516$ (5) Å, $c = 24.622$ (4) Å, $\beta = 99.02$ (1)°, $V = 6613$ (2) Å^3, $Z = 8$, R1 = 0.0789. Both **1**$[OTf]_2$ and **2**$[OTf]_2$ are soluble in water where they exhibit irreversible electrochemical oxidation and reduction. A fluorescence-monitored titration of a DNA solution containing **2**$[OTf]_2$ with ethidium bromide provides evidence that $\mathbf{2}^{2+}$ intercalates into DNA with a binding constant greater than 10^6 M^{-1}. DNA cleavage occurs when the DNA solutions containing **2**$[OTf]_2$ are photolyzed or treated with H_2O_2 or $K_2S_2O_8$.

Introduction

The intercalation of metal complexes into DNA and direct binding of metals with DNA base pairs has been a major focus in the study of bioinorganic chemistry. The study of such interactions is important for the development of new pharmaceuticals,[1] synthetic restriction enzymes,[2] and luminescent reporters for DNA.[3] The interaction of DNA with classical coordination compounds like $[Ru(phen)_3]^{2+}$, *cis*-platinum complexes, and simple hydrated metal cations has been a principal focus of research.[1b,4] However, the number of studies on organometallic complexes is very small (phen = bis(1,10-phenanthroline).[5] This is primarily the result of the low solubility and instability of many organometallic complexes in water. Furthermore, the need for buffered aqueous conditions in the pH range of 7−8 also complicates the situation.

Complexes containing the dipyrido[3,2-*a*:2′,3′-*c*]phenazine (dppz) ligand are noted for DNA intercalation.[6] Studies performed with $[Ru(bipy)_2(dppz)]^{2+}$ indicate comparable binding to both AT- and GC-rich DNA with an equilibrium binding constant of $>10^6$ M^{-1} (bipy = 2,2′-bipyridine).[7] The intercalative character of this binding to both B- and Z-DNA has also been established.[8] Ruthenium complexes containing dppz ligands exhibit enhanced photoluminescence and extended excited-state lifetimes when bound to DNA.[3,7] Molecular orbital calculations suggest that the LUMO of $[Ru(bipy)_2(dppz)]^{2+}$ is localized on the phenazine region of the dppz ligand.[9] Thus, the potential exists for photo-initiated electron transfer from the metal to a molecule of DNA as mediated through the phenazine region of dppz. Photoinduced DNA cleavage has been observed for a number of transition-metal complexes, including $[Rh(phen)_3]^{3+}$, $[Co(NH_3)_6]^{3+}$, and $[Ru(bipy)_3]^{2+}$. The quantum yields of DNA cleavage for these complexes range from 10^{-7} to 10^{-4} per DNA plasmid.[10] More recently, Shields and Barton reported sequence-specific DNA photocleavage by one of the enantiomers of $[Rh(en)_2phi]^{3+}$ (en = ethylenediamine, phi = 9,10-phenanthrenequinone diimine).[11] The efficiency of photocleavage processes is strongly affected by the absorption spectrum of the metal complex, as well as by the DNA binding affinity.

Herein we describe the chemistry of $[(\eta\text{-}C_5Me_5)Ru(NO)(bipy)][OTf]_2$ (**1**$[OTf]_2$) and $[(\eta\text{-}C_5Me_5)Ru(NO)(dppz)][OTf]_2$ (**2**$[OTf]_2$). These new water-soluble salts contain the robust $[(\eta\text{-}C_5Me_5)Ru(NO)]$ core that has been well-characterized in the realm of organometallic chemistry.[12,13] We provide evidence that $\mathbf{2}^{2+}$ intercalates into DNA and promotes DNA cleavage.

[⊗] Abstract published in *Advance ACS Abstracts,* June 15, 1996.

(1) (a) Hecht, S. M. *Acc. Chem. Res.* **1986**, *19*, 83. (b) Farrell, N. P. *Transition Metal Complexes as Drug and Chemotheraputic Agents.* Dordrecht, Boston, MA: Kluwer Academic Publishers, 1989.
(2) Barton, J. K. *Science* **1986**, *233*, 727.
(3) Hartshorn, R. M.; Barton, J. K. *J. Am. Chem. Soc.* **1992**, *114*, 5919.
(4) Pyle, A. M.; Rehmannm J. P.; Meshoyrer, R.; Kumar, C. V.; Turro, N. J.; Barton, J. K. *J. Am. Chem. Soc.* **1989**, *111*, 3051.
(5) (a) Smith, D. P.; Griffin, M. T.; Olmstead, M. M.; Maestre, M. F.; Fish, R. H. *Inorg. Chem.* **1993**, *32*, 4677. (b) Chen, H.; Maestre, M. F.; Fish, R. H. *J. Am. Chem. Soc.* **1995**, *117*, 3631, (c) Kickham, J. E.; Loeb, S. J.; Murphy, S. L. *J. Am. Chem. Soc.* **1993**, *115*, 7031.
(6) (a) Gupta, N.; Grover, N.; Neyhart, G. A.; Liang, W.; Singh, P.; Thorp, H. H. *Angew. Chem., Int. Ed. Engl.* **1992**, *31*, 1048. (b) Gupta, N.; Grover, N.; Neyhart, G. A.; Singh, P.; Thorp, H. H. *Inorg. Chem.* **1993**, *32*, 310.
(7) Friedman, A. E.; Chambron, J.; Sauvage, J.; Turro, N. J.; Barton, J. K. *J. Am. Chem. Soc.* **1990**, *112*, 4960.
(8) Friedman, A. E.; Kumar, C. V.; Turro, N. J.; Barton, J. K. *Nucleic Acids Res.* **1991**, *19*, 2595.
(9) (a) Fees, J.; Kaim, W.; Moscherosch, M.; Matheis, W.; Klima, J.; Krejcik, M.; Zalis, S. *Inorg. Chem.* **1993**, *32*, 166. (b) Amouyal, E.; Homsi, A.; Chambron, J.; Sauvage, J. *J. Chem. Soc. Dalton Trans.* **1990**, 1841.
(10) Fleisher, M. B.; Waterman, K. C.; Turro, N. J.; Barton, J. K. *Inorg. Chem.* **1986**, *25*, 3549.
(11) Shields, T. P.; Barton, J. K. *Biochemistry* **1995**, *34*, 15037.
(12) (a) Hubbard, J. L.; Morneau, A.; Burns, R. M.; Zoch, C. R. *J. Am. Chem. Soc.* **1991**, *113*, 9180. (b) Hubbard, J. L.; Morneau, A.; Burns, R. M.; Nadeau, O. W. *J. Am. Chem. Soc.* **1991**, *113*, 9176. (c) Burns, R. M.; Hubbard, J. L. *J. Am. Chem. Soc.* **1994**, *116*, 9514. (d) Svetlanova-Larsen, A.; Zoch, C. R.; Hubbard, J. L. *Organometallics*, in press.

S0020-1669(95)00743-9 CCC: $12.00

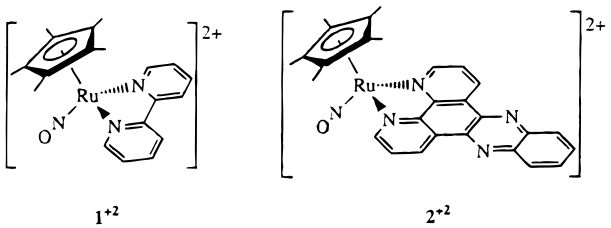

1^{+2} 2^{+2}

Results

Synthesis of 1[OTf]$_2$ and 2[OTf]$_2$. The addition of 2,2′-bipyridine to a solution of (η-C_5Me_5)Ru(NO)(OTf)$_2$[12d] in THF results in the precipitation of bright yellow microcrystalline **1**[OTf]$_2$. The addition of (η-C_5Me_5)Ru(NO)(OTf)$_2$ to a CH_2Cl_2 solution of dppz results in precipitation of the pale yellow dppz complex **2**[OTf]$_2$ (eq 1). Both compounds can be handled in air but are best stored in the dark at −10 °C to avoid darkening. Crystals suitable for X-ray crystallography are grown by the slow evaporation from CH_2Cl_2/toluene solutions.

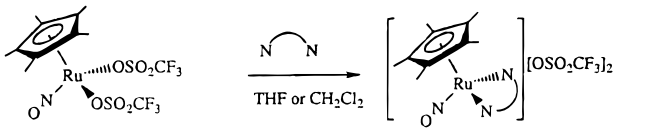

N N = bipy. dppz

1, 2 (1)

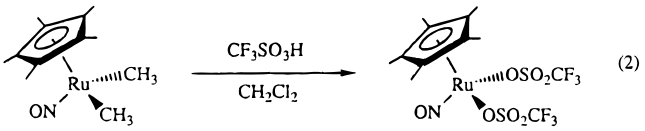

(2)

Both **1**[OTf]$_2$ and **2**[OTf]$_2$ are only slightly soluble in CH_2Cl_2. The complexes are only slightly soluble in Et_2O and THF and are essentially insoluble in aliphatic and aromatic solvents. They are moderately soluble without decomposition in H_2O as demonstrated by the recovery of analytically pure material upon removal of H_2O *in vacuo*. In solid KBr mulls, the complexes display strong ν_{NO} absorptions in the IR spectrum at 1846 cm^{-1} characteristic of a terminally bound NO ligand. In the ^1H and ^{13}C NMR spectra, both complexes display typical resonances for the (η-C_5Me_5) ligands as well as aromatic resonances that can be assigned to the bipy and dppz ligands. Both complexes display a single ^{19}F NMR resonance at δ −78.67 that is coincident with the ^{19}F signal from dissolved LiOTf. Aqueous solutions of **1**[OTf]$_2$ exhibit strong absorptions in the UV−visible spectrum at 284 and 322 nm with ϵ values of 9700 and 9400 M^{-1} cm^{-1} respectively. Similarly, complex **2**[OTf]$_2$ has intense absorptions at 286, 360, and 380 nm with ϵ values of 44 000, 14 000, and 13 000 M^{-1} cm^{-1}, respectively. Identical spectra are observed when **1**[OTf]$_2$ and **2**[OTf]$_2$ are dissolved in tris(hydroxymethyl)aminomethane/(ethylenedinitrilo)tetraacetic acid (TAE) buffer with no detectable changes observed over an 3 h period.

X-ray Crystallography. The crystallographic parameters and selected geometric data for **1**[OTf]$_2$ and **2**[OTf]$_2$ are summarized in Tables 1−3. The thermal ellipsoid plot showing the cation $\mathbf{1}^{2+}$ and nearest neighbor OTf^- ions is shown in Figure 1. The two independent cations found in the asymmetric unit of **2**[OTf]$_2$ are shown in Figure 2 (only the centroid of the (η-C_5Me_5) ring is shown for clarity). The two independent cationic complexes in **2**[OTf]$_2$ form pairs that stack via the dppz ligand with an interplanar separation of 3.5 Å (**A** in Figure 3). These pairs stack with a secondary interplanar 3.5 Å separation (**B**), leading to the extended array shown in Figure 3. The four OTf^- ions are closely associated with the stacked cations. Table 3 provides a summary of nonbonded OTf^- contacts to a variety of positions on the $\mathbf{2}^{2+}$ cations through both F and O atoms. For instance, the OTf^- ion containing the S(2) atom bridges via its O(7) and O(6) atoms between the dppz ligands on a pair of $\mathbf{2}^{2+}$ cations containing Ru(1) and Ru(2) (Figure 2).

The immediate coordination sphere of the cations $\mathbf{1}^{2+}$ and $\mathbf{2}^{2+}$ each exhibit a three-legged piano stool geometry with an essentially planar and symmetrically bound (η-C_5Me_5) ligand lying at ca. 42° relative to the plane of the bipy or dppz ligands. ∠Ru−N−O ranges from 163 to 169° and the metallacyclic moiety [Ru−N−C−C−N] deviates from planarity by only 0.04−0.05 Å in each case.

Photolysis of 1[OTf]$_2$ and 2[OTf]$_2$. Exposure of aqueous solutions of either **1**[OTf]$_2$ or **2**[OTf]$_2$ to broad-band light causes the gradual disappearance of the ^1H NMR signals from cation

Table 1. Crystal Data for Complexes **1**[OTf]$_2$ and **2**[OTf]$_2$

	1[OTf]$_2$	**2**[OTf]$_2$
formula	$C_{22}H_{23}F_6N_3O_7RuS_2$	$C_{30}H_{25}F_6N_5O_7RuS_2$
fw	720.6	846.7
space group	$P2_1/c$	$P2_1/c$
a, Å	11.553(4)	8.911(2)
b, Å	16.517(5)	30.516(5)
c, Å	14.719(4)	24.622(4)
β, deg	94.01(2)	99.02(1)
V, Å^3	2802(2)	6613(2)
Z	4	8
d_{calc}, g/cm^3	1.708	1.701
μ(Mo Kα), mm^{-1}	0.795	0.689
temp, K	298	298
scan method	$\theta-2\theta$	ω
data collcn range (2θ), deg	3−45	3−45
no. of unique data/params	3654/371	8650/914
refnmt method	least-squares on F^2	least-squares on F^2
R1[a]	0.0698	0.0789
wR2[b]	0.1094	0.2227
GOF	1.043	1.124

[a] $R1 = \sum||F_o| - |F_c|/\sum|F_o|$. [b] $wR2 = |\sum[w(F_o^2 - F_c^2)]^2]/\sum[w(F_o^2)^2]]^{1/2}$.

Table 2. Selected Geometric Data for **1**[OTf]$_2$

	Bond Lengths, Å		
Ru−N(1)	1.80(1)	O(2)- - -N(1)	2.93
Ru−N(2)	2.096(9)	O(2)- - -N(3)	3.09
Ru−N(3)	2.079(9)	O(3)- - -N(1)	3.78
N(1)−O(1)	1.13(1)	O(3)- - -N(2)	3.23
Ru−Cp[a]	1.87	O(6)- - -C(26)	3.58
		O(6)- - -C(36)	3.37
	Bond Angles, deg		
N(1)−Ru−N(2)	98.7(5)	Ru−N(2)−C(21)	116.6(7)
N(1)−Ru−N(3)	101.4(4)	Ru−N(3)−C(31)	116.0(8)
N(2)−Ru−N(3)	77.0(4)	Cp[a]−Ru−N(1)	122
Ru−N(1)−O(1)	166(1)	Cp[a]−Ru−N(2)	126
N(2)−C(21)−C(31)	115(1)	Cp[a]−Ru−N(3)	122
N(3)−C(31)−C(21)	115(1)		
	Planes, Mean Deviation from Planarity, Å		
plane 1: Ru−N(1)−C(21)−C(31)−N(3)			0.04
plane 2: C(1)−C(2)−C(3)−C(4)−C(5)			0.01
	Angles between Planes, deg		
plane 1:plane 2	42		

[a] Cp = centroid of η-C_5Me_5 ligand.

(13) (a) Seidler, M. D.; Bergman, R. G. *J. Am. Chem. Soc.* **1984**, *106*, 6110. (b) Chang. J.; Bergman, R. G. *J. Am. Chem. Soc.* **1987**, *109*, 4298. (c) Chang. J.; Seidler, M. D.; Bergman, R. G. *J. Am. Chem. Soc.* **1989**, *111*, 3258. (d) Brookhart, M. Sabo-Etienne, S. *J. Am. Chem. Soc.* **1991**, *113*, 2777.

Table 3. Selected Geometric Data for **2**[OTf]$_2$

Bond Lengths, Å			
Ru(1)−N(1)	1.78(2)	N(8)−C(57)	1.41(2)
Ru(1)−N(2)	2.11(1)	Ru(2)−Cp[a]	1.88
Ru(1)−N(3)	2.10(1)	F(1)- - -C(29)	3.49
N(1)−O(1)	1.14(2)	F(1)- - -F(4)	2.88
N(2)−C(37)	1.32(2)	F(2)- - -C(15)	3.34
N(3)−C(38)	1.38(2)	F(8)- - -C(42)	3.14
Ru(1)−Cp[a]	1.87	F(10)--C(19)	3.80
Ru(2)−N(6)	1.78(2)	O(6)- - -C(23)	3.24
Ru(2)−N(7)	2.12(1)	O(7)- - -C(56)	3.16
Ru(2)−N(8)	2.09(1)	O(8)- - -C(18)	3.29
N(6)−O(2)	1.14(2)	O(9)- - -C(35)	3.01
N(7)−C(58)	1.35(2)	O(11)- -C(49)	3.91
Bond Angles, deg			
N(1)−Ru(1)−N(2)	102.8(6)	N(6)−Ru(2)−N(7)	101.6(5)
N(1)−Ru(1)−N(3)	99.9(5)	N(6)−Ru(2)−N(8)	99.0(6)
N(2)−Ru(1)−N(3)	76.6(5)	N(7)−Ru(2)−N(8)	77.5(5)
Ru(1)−N(1)−O(1)	170(1)	Ru(2)−N(6)−O(2)	163(1)
Ru(1)−N(2)−C(37)	116(1)	Ru(2)−N(7)−C(58)	115(1)
Ru(1)−N(3)−C(38)	116(1)	Ru(2)−N(8)−C(57)	115(1)
Cp[a]−Ru(1)−N(1)	123	Cp[a]−Ru(2)−N(6)	122
Cp[a]−Ru(1)−N(2)	122	Cp[a]−Ru(2)−N(7)	124
Cp[a]−Ru(1)−N(3)	123	Cp[a]−Ru(2)−N(8)	124

Planes, Mean Deviation from Planarity, Å

plane 1:	Ru(1)−N(2)−C(37)−C(38)−N(3)	0.04
plane 2:	C(1)−C(2)−C(3)−C(4)−C(5)	0.01
plane 3:	Ru(2)−N(7)−C(58)−C(57)−N(8)	0.05
plane 4:	C(6)−C(7)−C(8)−C(9)−C(10)	0.01

Angles between Planes, deg

plane 1:plane 2	42
plane 3:plane 4	42

[a] Cp = centroid of C_5Me_5 ring.

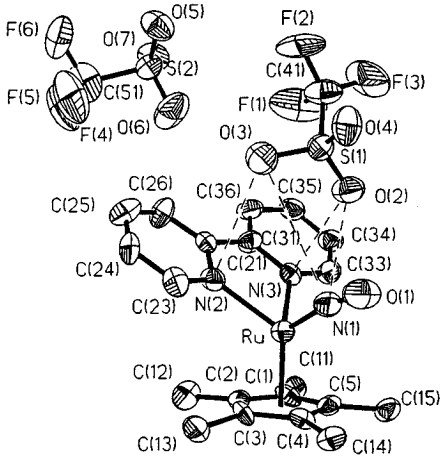

Figure 1. Thermal ellipsoid plot (30% probability level) and atom numbering scheme for **1**[OTf]$_2$. Dashed lines indicate closest approach of the OTf^- ion (see Table 2).

$\mathbf{1}^{2+}$ over a 36 h period with no identifiable new products. The similar loss of the ^{1}H NMR signals of $\mathbf{2}^{2+}$ occurs over a 17 h period. The photolysis of **2**[OTf]$_2$ in TAE buffer for 90 min results in the broadening and ca. 10% loss of intensity of the UV−vis absorptions of $\mathbf{2}^{2+}$. The EPR spectra of photolyzed samples of **1**[OTf]$_2$ and **2**[OTf]$_2$ at 14 K do not show the presence of free NO. Photolysis of **1**[OTf]$_2$ or **2**[OTf]$_2$ in the presence of the spin-trapping reagent DMPO (5,5-dimethyl-1-pyrroline *N*-oxide) results in the appearance of a quartet EPR signal (g = 2.005, A = 14.9 G). This signal increases in intensity as the photolysis time increases.

Electrochemical Behavior of 1[OTf]$_2$. In CH_3CN solution, **1**[OTf]$_2$ undergoes a partially reversible oxidation at $E_{1/2}$ = −0.05 V at sweep rates as low as 0.1 V/s. No other anodic peaks are observed in CH_3CN. When **1**[OTf]$_2$ is reduced in

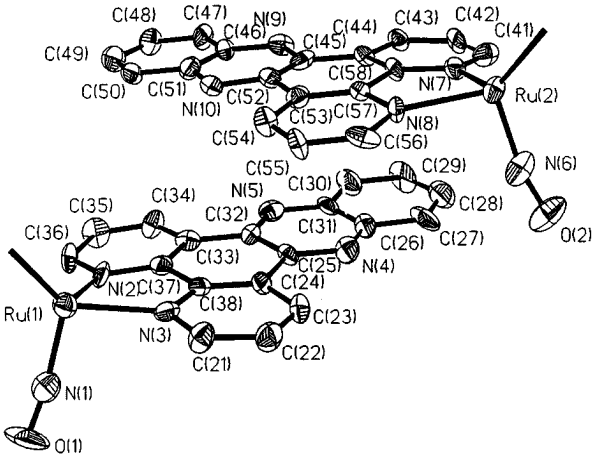

Figure 2. Thermal ellipsoid plot (30% probability level) and atom numbering scheme for the independent cations $\mathbf{2}^{2+}$ (η-C_5Me_5 ligand and CF_3SO_3 anions omitted for clarity).

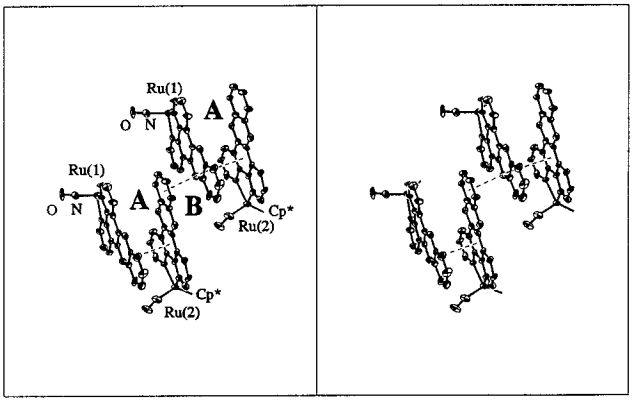

Figure 3. Stereoview of the crystal packing of the cations $\mathbf{2}^{2+}$ (η-C_5Me_5 ligand and CF_3SO_3 anions omitted for clarity). **A** is the 3.5 Å interplanar separation between the independent cations; **B** is the interplanar separation between the pairs of cations.

CH_3CN, two reversible cathodic waves are observed at $E_{1/2}$ = −0.69 V and $E_{1/2}$ = −1.52 V. A partially reversible wave at $E_{1/2}$ = −1.81 V appears as a shoulder near the background limit of the solvent.

Aqueous solutions of **1**[OTf]$_2$ exhibit an irreversible oxidation at E_{pa} = −0.04 V at sweep rates up to 300 V/s. A second irreversible oxidation is detected at E_{pa} = 0.29 V. The reduction of **1**[OTf]$_2$ in water gives an irreversible cathodic peak at E_{pa} = −0.86 V. A second irreversible cathodic peak is observed at E_{pa} = −1.38 V.

Electrochemical Behavior of 2[OTf]$_2$. In pure CH_3CN, **2**[OTf]$_2$, undergoes a single partially reversible oxidation at $E_{1/2}$ = −0.02 V and an irreversible reduction at E_{pc} = −0.69 V followed by a partially reversible reduction with $E_{1/2}$ = −1.00 V. In a 9:1 mixture of H_2O/CH_3CN, **2**[OTf]$_2$ shows an irreversible oxidation at E_{pa} = −0.21 V and a second irreversible oxidation at E_{pa} = 0.40 V. In H_2O, **2**[OTf]$_2$ exhibits a single irreversible reduction wave at E_{pc} = −1.11 V.

DNA Interactions. When an H_2O solution of **2[OTf]$_2$** is added to the supercoiled DNA plasmid pLCS792, a change in DNA mobility is detected by gel electrophoresis on an agarose gel. At room temperature, a single broad band appears that is less mobile than the untreated plasmid control (see Figure 4). As the ratio of metal complex to DNA is increased, this single band becomes less mobile and more diffuse. The addition of aqueous **1**[OTf]$_2$ or $RuCl_3$ to DNA solutions results in gel bands that are indistinguishable from untreated plasmid bands (Figure 5, lanes 3 and 5). When solutions of **2**[OTf]$_2$ and plasmid DNA

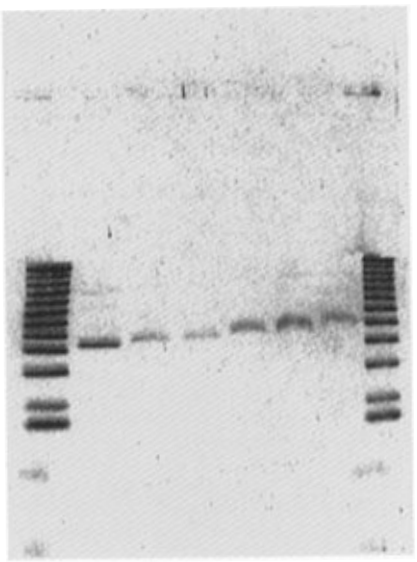

Figure 4. Photograph of a 0.8% agarose gel showing the interaction of **2**[OTf]$_2$ with plasmid pLCS792: (1) untreated plasmid; (2) 14 μM **2**[OTf]$_2$ plasmid; (3) 19 μM **2**[OTf]$_2$ + plasmid; (4) 24 μM **2**[OTf]$_2$ + plasmid; (5) 28 μM **2**[OTf]$_2$ + plasmid; (6) 33 μM **2**[OTf]$_2$ + plasmid. The nucleotide concentration was 30 μM. All samples were incubated for 30 min at 25 °C. Outer lanes show DNA ladders used for reference purposes.

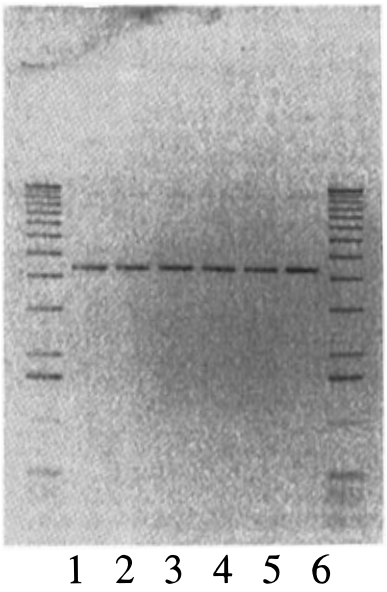

Figure 5. Photograph of a 0.8% agarose gel showing control experiments on plasmid pLCS792: (1) plasmid alone; (2) plasmid photolyzed 25 min; (3) plasmid + 30 μM **1**[OTf]$_2$; (4) plasmid + 30 μM **1**[OTf]$_2$ photolyzed 25 min; (5) plasmid + 30 μM $RuCl_3$; (6) plasmid + 30 μM $RuCl_3$, photolyzed 25 min. The nucleotide concentration was 30 μM. Lanes 1, 3, and 5 were incubated for 30 min at 25 °C. Outer lanes show DNA ladders used for reference purposes.

are titrated with an ethidium bromide solution, the fluorescence intensity of ethidium decreases as the concentration of **2**[OTf]$_2$ is increased. Application of the Scatchard equation to this data yields the lines shown in Figure 6.[14]

DNA Cleavage Chemistry. When a solution of DNA and **2**[OTf]$_2$ is photolyzed with broad-band light, the less mobile band corresponding to nicked circular DNA intensifies and the diffuse band disappears (Figure 7). If the solution is photolyzed

(14) Jennette, K. W.; Lippard, S. J.; Vassiliades, G. A.; Bauer, W. R. *Proc. Nat. Acad. Sci. U.S.A.* **1974**, *71*, 3839.

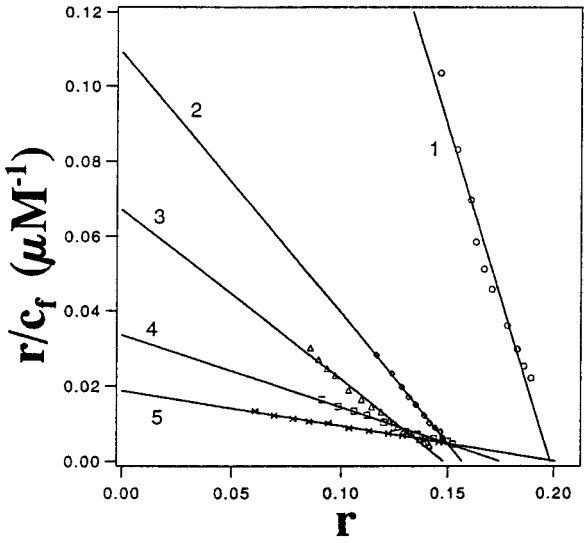

Figure 6. Fluorescence Scatchard plots of ethidium bromide (concentration 0.25 to 80 μM) bound to plasmid pLCS972 (7.4 μM nucleotide) in TAE buffer (line 1) and in increasing concentrations of **2**[OTf]$_2$: line 2, $c_M = 0.4$ μM; line 3, $c_M = 0.8$ μM; line 4, $c_M = 1.6$ μM; line 5, $c_M = 3.2$ μM. K_M/K_{Etd} for these plots is 3.3.

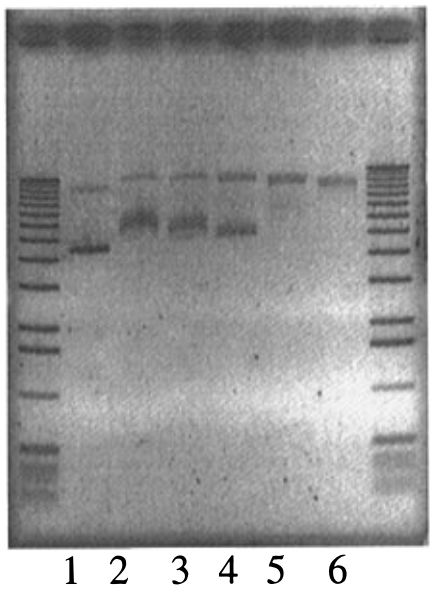

Figure 7. Photograph of a 0.8% agarose gel showing the photolysis of **2**[OTf]$_2$ with plasmid pLCS792: (1) untreated plasmid; (2) **2**[OTf]$_2$ + plasmid, 0 min photolysis; (3) **2**[OTf]$_2$ + plasmid, 2 min photolysis; (4) **2**[OTf]$_2$ + plasmid, 5 min photolysis; (5) **2**[OTf]$_2$ + plasmid, 10 min photolysis; (6) **2**[OTf]$_2$ + plasmid, 20 min photolysis. The nucleotide concentration was 30 μM and the concentration of **2**[OTf]$_2$ was 30 μM. Outer lanes show DNA ladders used for reference purposes.

for longer than 20 min, the single band shown in Figure 7 (lane 6) gradually disappears. After 40 min of photolysis, no DNA fragments can be detected. Addition of 5 equiv of H_2O_2 or $K_2S_2O_8$ followed by incubation at 40 °C for 1 h also results in the appearance of a less mobile band when **2**[OTf]$_2$ is present (Figure 8, lanes 1−2). When solutions of **2**[OTf]$_2$ are photolyzed and then subsequently added to DNA in the dark, one diffuse band is observed (Figure 9, lane 3). Subsequent photolysis of this mixture causes a less mobile band to appear. (Figure 9, lane 4) The appearance of the less mobile band is not affected when DMPO (80 mM) is added to the reaction mixtures. Photolysis of untreated DNA plasmid does not produce additional bands (Figure 5, lane 2). Similar results are observed for the photolysis of DNA treated with **1**[OTf]$_2$ and $RuCl_3$ (Figure 5, lanes 4 and 6).

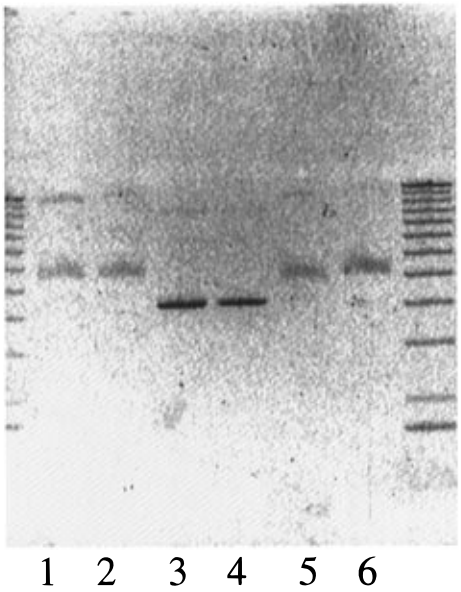

Figure 8. Photograph of a 0.8% agarose gel showing the reaction of H_2O_2 and $K_2S_2O_8$ with **2**$[OTf]_2$ and plasmid pLCS792: (1) 40 μM **2**$[OTf]_2$ + plasmid + 120 μM H_2O_2; (2) 40 μM **2**$[OTf]_2$ + plasmid + 120 μM $K_2S_2O_8$; (3) plasmid + 120 μM H_2O_2; (4) plasmid + 120 μM $K_2S_2O_8$; (5) 40 μM **2**$[OTf]_2$ + plasmid + 240 μM H_2O_2; (6) 40 μM **2**$[OTf]_2$ + plasmid + 240 μM $K_2S_2O_8$. The nucleotide concentration was 30 μM. Lanes 1−4 were incubated for 1 h at 40 °C; lanes 5−6, were incubated for 1 h at 25 °C. Outer lanes show DNA ladders used for reference purposes.

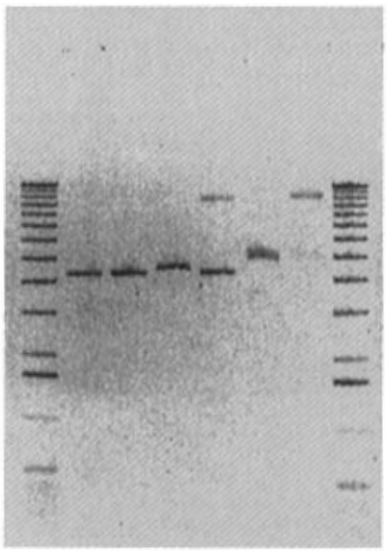

Figure 9. Photograph of a 0.8% agarose gel showing the effect of prephotolysis of **2**$[OTf]_2$: (1) plasmid alone; (2) plasmid, photolyzed 25 min; (3) plasmid + 30 μM prephotolyzed **2**$[OTf]_2$; (4) plasmid + 30 μM prephotolyzed **2**$[OTf]_2$ photolyzed 25 min; (5) plasmid + 30 μM **2**; (6) plasmid + 30 μM **2**$[OTf]_2$ photolyzed 25 min. The nucleotide concentration was 30 μM. Lanes 1, 3, and 5 were incubated for 30 min at 25 °C. Outer lanes show DNA ladders used for reference purposes.

Treatment of the pLCS792 plasmid with the restriction enzyme *BamH I* yields a single sharp band (Figure 10, lanes 1−2). Addition of the DNA cleavage enzyme DNase to the same plasmid yields two bands, corresponding to the unchanged plasmid and its nicked circular form (Figure 10, lanes 4−5).

Discussion

Characteristics of 1[OTf]$_2$ and 2[OTf]$_2$. The OTf^- salts of $\mathbf{1}^{2+}$ and $\mathbf{2}^{2+}$ exhibit similar solubilities in polar organic solvents but **1**$[OTf]_2$ is somewhat more soluble in H_2O than is **2**$[OTf]_2$. The cations $\mathbf{1}^{2+}$ and $\mathbf{2}^{2+}$ show characteristic ^1H and ^{13}C NMR signals of the η-C_5Me_5 ligand in H_2O with no signs of decomposition over several days. The complexes are similarly stable in a TAE buffer solution.

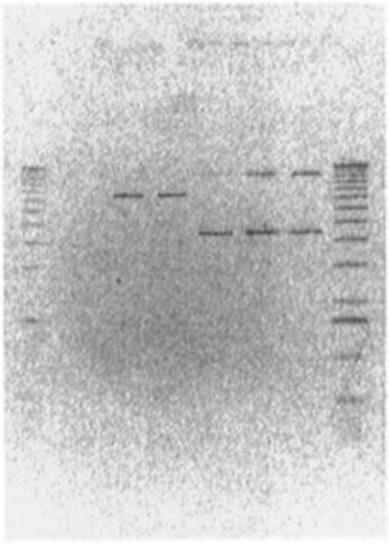

Figure 10. Representation of an 0.8% agarose gel showing the reaction of pLCS792 with *BamH I* and DNase: (1 and 2) plasmid + *BamH I* incubated at 37 °C for 30 min; (3) plasmid + DNase incubated at 25 °C for 5 min; (4) plasmid + DNase incubated at 25 °C for 10 min; (5) plasmid + DNase incubated at 25 °C for 20 min. Right lane shows a reference ladder.

The cations $\mathbf{1}^{2+}$ and $\mathbf{2}^{2+}$ possess very similar coordination environments. The angles and distances of the [η-C_5Me_5)Ru-(NO)] moieties are remarkably constant within experimental error. The consistency of the angle between the planes of the bipy or dppz ligands relative to the planes of the corresponding η-C_5Me_5 ligands shows that the size of the heterocyclic ligand has no effect on the local coordination geometry. However, the large dppz ligand does give rise to extensive stacking of the cations in the unit cell. This presumably is the result of $\pi-\pi$ intermolecular interactions.[15] A similar stacking in the structure of $[Ru(OH_2)(dppz)(tpy)]^{2+}$ has been observed (tpy = 2,2′:6′,2″-terpyridine).[6a] No similar stacking is observed in the case of **1**$[OTf]_2$.

Redox Chemistry. With the exception of the reduction of $\mathbf{2}^{2+}$, the electrochemical behavior of **1**$[OTf]_2$ and **2**$[OTf]_2$ is at least partially reversible in CH_3CN. The oxidation of cation $\mathbf{2}^{2+}$ occurs at only 0.03 V more positive than the oxidation of $\mathbf{1}^{2+}$. On the basis of the electrochemical data obtained in CH_3CN, changing the bipy ligand to dppz does not greatly affect the redox potentials but does make $\mathbf{2}^{2+}$ unstable to reduction.

Both **1**$[OTf]_2$ and **2**$[OTf]_2$ react with chemical oxidants in H_2O, but the paramagnetic nature of the putative oxidation products $\mathbf{1}^{3+}$ and $\mathbf{2}^{3+}$ apparently makes them silent in the NMR spectrum. EPR measurements thus far have also failed to detect their presence. In H_2O or H_2O/CH_3CN mixtures, all of the electrochemical events are irreversible. Thus, a comparison of the redox properties of $\mathbf{1}^{2+}$ and $\mathbf{2}^{2+}$ in H_2O is less meaningful. Similar irreversibility in the electrochemistry of the related $[Ru(bipy)_2(dppz)]^{2+}$ complex has been reported by Fees and Kaim.[9] It is possible that H_2O rapidly intercepts the products generated in the electrochemical oxidation or reduction of $\mathbf{1}^{2+}$ or $\mathbf{2}^{2+}$.

Interactions of $\mathbf{2}^{2+}$ with DNA. The electrophoresis bands observed when supercoiled DNA is treated with 14−40 μM

(15) Hunter, C. A.; Sanders, J. K. M. *J. Am. Chem. Soc.* **1990**, *12*, 5525.

$\mathbf{2}^{2+}$ in TAE buffer (Figure 4) indicate that an interaction is occurring. This interaction can not solely be due to the +2 charge on the complex because $\mathbf{1}^{2+}$ does not produce the same effect. The Scatchard plots show the apparent binding constant of ethidium bromide to decrease as c_M is increased (slope = $-K_{obs}$). This indicates that $\mathbf{2}^{2+}$ is in competition with ethidium bromide for binding sites on DNA.[16] From the slopes of the lines in Figure 7 for the corresponding concentrations of $\mathbf{2}^{2+}$, we can estimate that $\mathbf{2}^{2+}$ has a binding constant for DNA that is $(1.5-2.0) \times 10^6$ M^{-1}, i.e. 3−4 times that of ethidium bromide.[14] Consistent with previous studies, the direct competition of $\mathbf{2}^{2+}$ with ethidium bromide infers that $\mathbf{2}^{2+}$ binds to supercoiled DNA in an intercalative fashion.[3,6−8] The variation of the *x*-intercept in the Scatchard plots for $\mathbf{2}^{2+}$ shows that a covalent interaction between $\mathbf{2}^{2+}$ and DNA cannot be completely ruled out. However, the expected loss of a ligand that would presumably precede a covalent interaction is not observed by NMR spectroscopy.

The absence of any interaction between $\mathbf{1}^{2+}$ and DNA contrasts with intercalative *cis*-$[Pt(bipy)X_2]$ complexes and the surface-bound $[Ru(bipy)_3]^{2+}$.[17,18] Studies have shown that the bipy ligand does not intercalate when bound to an octahedral metal center.[4] The surface binding is due to electrostatic attraction and is generally weaker than intercalative binding. Intercalation in the case of the square planar Pt(bipy) systems is possible because of lower steric demands. The larger steric demands of $\mathbf{1}^{2+}$ could be expected to thwart intercalation, but the reason for the apparent lack of surface binding is not clear. It is possible that the shape of the complex prevents binding on the surface of DNA. It is also possible that $\mathbf{1}^{2+}$ does not bind strongly enough to DNA to cause changes in the agarose gels.

The behavior of the $\mathbf{2}^{2+}$·DNA association complex under photolysis is consistent with a "nicking" reaction where a single strand of DNA is severed. In some of the photolysis experiments, a faint band corresponding to nicked DNA can be seen in the control lane (Figure 5, lane 1). This band grows in intensity as the photolysis progresses and is similar to the DNA nicking caused by DNase (Figure 10). A much sharper band representing specific cleavage at a single site occurs when the pLCS972 plasmid is treated with the restriction enzyme *BamH I* (Figure 10).

Summary. While the precise mechanism of the DNA cleavage reaction is still unknown, it is possible to deduce that nicking results from the close proximity of $\mathbf{2}^{2+}$ to the DNA strand. The lack of DNA cleavage when a photolyzed solution of $\mathbf{2}[OTf]_2$ is subsequently added to DNA in the dark argues against the action of photolysis byproducts resulting from $\mathbf{2}[OTf]_2$ alone. The lack of DNA cleavage in the presence of $RuCl_3$ rules against the action of a simple Ru^{2+} ion. The ability of DMPO to trap OH radicals when $\mathbf{1}^{2+}$ or $\mathbf{2}^{2+}$ are photolyzed in the absence of DNA shows that DNA strand breaks may result from the rapid action of $OH^{\bullet}$.[19] However, the failure of DMPO to trap any radicals when $\mathbf{1}^{+1}$ or $\mathbf{2}^{2+}$ are present with DNA indicates that any radical species do not escape from the vicinity of the metal complex. The observation that DNA cleavage is not observed when $\mathbf{1}^{2+}$ is present is consistent with a requirement for binding between the complex and DNA. The production of singlet oxygen could be responsible for DNA strand breaks similar to that observed in the photocleavage of DNA by $[Ru(phen)_3]^{2+}$.[10]

The exploration of a possible electron-transfer process from the metal complex to DNA will require a complete photophysical analysis of $\mathbf{2}[OTf]_2$. We are hopeful that our continuing study of aqueous organometallic chemistry will provide more insight into this important area of bioinorganic reactivity.

Experimental Section

All reactions were carried out using standard Schlenk techniques. The nitrogen reaction atmosphere was purified by passing through scavengers for H_2O (Aquasorb, Mallinkrodt) and oxygen (Catalyst R3-11, Chemical Dynamics, South Plainfield, NJ). Reagent grade solvents were dried over appropriate drying agents and saturated with N_2 prior to use.[20] The H_2O was purified and deionized (NANO-pure Ultrapure Water System) and saturated with N_2 gas prior to use. The bipy ligand was used as received from Aldrich, and the dppz ligand was synthesized using a literature method.[21] *BamH I* and DNase were used as received from Sigma. The plasmid pLCS792 was obtained from Dr. Lance Seefeldt and purified as described in the literature.[22] High-strength, analytical grade agarose was used as received from Bio-Rad. Agarose gel electrophoresis was performed at 55 V using a BRL Horizon 58 Horizontal Gel Electrophoresis System with a Bio-Rad Model 3000Xi computer-controlled power supply. Infrared spectra were measured at 2.0 cm^{-1} resolution on a Mattson Polaris-Icon FT Spectrophotometer. ^1H, ^{13}C, and ^{19}F NMR spectra were recorded on a Bruker 400 MHz spectrometer; the ^1H and ^{13}C NMR spectra were referenced to residual solvent peaks, and the ^{19}F NMR spectra were referenced externally to CCl_3F (δ 0.0)[20] or internally to 3,5-bis(trifluoromethyl)benzene (δ −63.20 in $CDCl_3$). NMR spectra in H_2O were measured using solvent presaturation techniques and were shimmed and referenced to the signals from $CDCl_3$ sealed inside a 1.5 mm capillary located concentrically inside the 5-mm NMR tube. EPR measurements were made at 14 and 298 K on a Bruker ESP 300E EPR spectrometer. DMPO was used as received from Sigma. UV−visible spectra were recorded on an HP8452a diode array spectrophotometer. Fluorescence measurements were made in a 1 cm quartz cell on a Gilford Fluoro IV spectrofluorometer. Single-crystal X-ray crystal analyses were performed on a Siemens P4 autodiffractometer. Photolyses were performed using a medium pressure 250 W Hg lamp (Hanovia) encased in a H_2O-cooled sleeve. Samples in 5-mm Pyrex NMR tubes, 4-mm quartz EPR tubes, or polypropylene microcentrifuge tubes were held vertically 10 cm from the lamp for the times designated. Combustion analysis was performed by Atlantic Microlab, Inc., Norcross, GA.

Electrochemical Measurements. Cyclic voltammetry was performed using a JAS Instrument Systems Model J-1600-B potentiostat driven by an external Hewlett-Packard 3314A function generator.[23] The signals were filtered with a Stanford Research Systems Inc. Model SR640 dual-channel low-pass filter before they were fed to a Nicolet Model 310 digital oscilloscope and processed by a personal computer. To reduce periodic noise, sequential scans at the selected sweep rate, sweep range and, trigger intervals were collected and averaged.[24,25] Positive *IR* compensation was employed. The following conditions were used for measurements in CH_3CN solvent: working electrode was a Pt disk electrode (d = 0.8 mm); counter-electrode was a Pt wire; reference electrode was a Ag wire in 0.01 M $AgNO_3$ in CH_3CN;[26] supporting electrolyte was 0.1 M Bu_4NPF_6; redox potentials in CH_3CN were referenced against the ferrocene/ferrocenium couple and then converted to the NHE scale. The following conditions were used for measurements in H_2O: working electrode was a Au disk electrode (d = 0.6 mm); counterelectrode was a Pt wire; the reference electrode was Ag/AgCl in a 3 M KCl solution and is referenced as 0.193 V vs

(16) Lippard, S. J. *Acc. Chem. Res.* **1978**, *11*, 211.
(17) Kelly, J. M.; Tossi, A. B.; McConnell, D. J.; Ohuigin, C. *Nucleic Acids Res.* **1985**, *13*, 6017.
(18) Howe-Grant, M.; Wu, K. C.; Bauer, W. R.; Lippard, S. J. *Biochemistry* **1976**, *15*, 4339.
(19) Buettner, G. R. The Spin-trapping of Superoxide and Hydroxyl Free Radicals. In *Superoxide Dismutase*; Oberly, L. W., Ed.; CRC Press: Boca Raton, FL, 1982; Vol. 2.
(20) Gordon, A. J.; Ford, R. A. *The Chemist's Companion*; John Wiley & Sons: New York, 1972; pp 25, 433.
(21) Dickeson, J. E.; Summers, L. A. *Aust. J. Chem.* **1970**, *23*, 1023.
(22) Mortensen, L. E.; Seefeldt, L. C. *Protein Sci.* **1993**, *2*, 93.
(23) Norrsell, F.; Handoo, K. L.; Parker, V. D. *J. Org. Chem.* **1993**, *58*, 4929.
(24) Lasson, E.; Parker, V. D. *Anal. Chem.* **1990**, *62*, 412.
(25) Moe, N. S. *Anal. Chem.* **1974**, *46*, 968.
(26) Kolthoff, I. M.; Chantooni, M. K. *J. Phys. Chem.* **1972**, *76*, 2024.

NHE; supporting electrolyte was 0.1 M $NaBF_4$. The value of the electrode potential for the ferrocene/ferrocenium couple is 0.527 V vs NHE.[21] All measurements were made under an argon atmosphere on 0.5 mM samples. The $E_{1/2}$ value is taken to be the midpoint between the anodic and cathodic CV peaks. The E_{pa} and E_{pc} values were taken as the peak value(s) in the anodic and cathodic scans, respectively.

Preparation of (η-C_5Me_5)Ru(NO)(OTf)$_2$. Triflic acid (1.60 mL, 18.08 mmol, 2.16 equiv) was added dropwise to a stirred solution of (η-C_5Me_5)Ru(NO)Me_2[13c] (2.48 g, 8.37 mmol) in 80 mL CH_2Cl_2. The solution color changed from deep red to purple with gas evolution. After 1 h of vigorous stirring, the solution volume was reduced to ca. 10 mL, and 60 mL of dry diethyl ether was added to precipitate the product. The nearly colorless supernatent solution was decanted away and the product dried under vacuum, giving 4.68 g (8.29 mmol, 99%) of (η-C_5Me_5)Ru(NO)$(OTf)_2$ as a purple microcrystalline powder. ^{1}H NMR (CH_2Cl_2): δ 1.88 (s, (η-$C_5(CH_3)_5$)). ^{13}C{^{1}H} NMR (CH_2Cl_2): δ 119.4 (q, OSO_2CF_3, J_{CF} = 318.4 Hz); 113.9 ($C_5(CH_3)_5$); 10.1 ($C_5(CH_3)_5$). ^{19}F{^{1}H} NMR (CH_2Cl_2): δ −76.02 (s, CF_3SO_3). IR (CH_2Cl_2): ν_{NO} 1848 cm^{-1} (vs). Mp: 209−211 °C. Anal. Calcd for $C_{12}H_{15}F_6NO_7RuS_2$: C, 25.53; H, 2.68; N, 2.48; Found: C, 25.05; H, 2.75; N, 2.43.

Preparation of [(η-C_5Me_5)Ru(NO)(bipy)][OTf]$_2$, 1[OTf]$_2$. To a solution prepared from (η-C_5Me_5)Ru(NO)$(OTf)_2$ (0.20 g, 0.360 mmol) in 20 mL of THF was added 2,2′-bipyridine (67 mg, 0.43 mmol) dissolved in 10 mL of THF. The color immediately changed from purple to yellow with the development of a yellow precipitate. After 30 min of stirring, the supernatent liquid was decanted away and discarded to leave **1**[OTf]$_2$ (0.27 g, 0.35 mmol, 97%) as a bright yellow solid after drying under vacuum. ^{1}H NMR (DMSO-d_6): δ 1.83 (s, 15H, (η-C_5Me_5)); 7.99 (t, 2H, $^3J_{H-H}$ = 7 Hz); 8.61 (t, 2H, $^3J_{H-H}$ = 8 Hz); 8.77 (d, 2H, $^3J_{H-H}$ = 6 Hz); 8.96 (d, 2H, $^3J_{H-H}$ = 8 Hz). ^{13}C NMR (DMSO-d_6): δ 155.7, 143.4, 129.0, 125.5 (bipy); 113.1 ($C_5(CH_3)_5$); 8.92 ($C_5(CH_3)_5$). ^{19}F NMR (H_2O): δ −78.67; IR (KBr, cm^{-1}): ν_{NO} 1846 (vs). UV−vis (H_2O): λ_{max} 284 nm (ϵ = 9700 cm^{-1} M^{-1}), 322 nm (ϵ = 9400 cm^{-1} M^{-1}). Mp: 225 °C dec. Anal. Calcd for $C_{22}H_{23}F_6N_3O_7RuS_2$ (M_r 720.6): C, 36.67; H, 3.22; N, 5.83; Found: C, 36.83; H, 3.20; N, 5.76.

Preparation of [(η-C_5Me_5)Ru(NO)(dppz)][OTf]$_2$, 2[OTf]$_2$. To a solution of dppz (0.084 g, 0.30 mmol) in 15 mL CH_2Cl_2 was quickly added (η-C_5Me_5)Ru(NO)$(OTf)_2$ (0.163 g, 0.29 mmol) dissolved in 10 mL of CH_2Cl_2. The initial purple color changed to yellow with the separation of a yellow precipitate. After 1 h the supernatent liquid was decanted away and the resulting pale yellow powder was dried under vacuum to give **2**[OTf]$_2$ (162 mg, 0.19 mmol, 66%). Recrystallization from CH_2Cl_2 and toluene produced orange crystals suitable for elemental analysis and X-ray crystallography. ^{1}H NMR (D_2O): δ 1.99 (s, 15H, (η-C_5Me_5)); 8.22 (dd, 2H, $^1J_{H-H}$ = 7 Hz, $^3J_{H-H}$ = 3 Hz); 8.45 (dd, 2H, $^1J_{H-H}$ = 5 Hz, $^1J_{H-H}$ = 8 Hz); 8.56 (dd, 2H, $^1J_{H-H}$ = 7 Hz, $^3J_{H-H}$ = 3 Hz); 9.18 (dd, 2H, $^1J_{H-H}$ = 5 Hz, $^3J_{H-H}$ = 1 Hz); 10.12 (dd, 2H, $^1J_{H-H}$ = 8 Hz, $^3J_{H-H}$ = 1 Hz). ^{13}C NMR (DMSO-d_6): δ 157.5, 150.3, 142.1, 139.2, 138.6, 133.1, 129.5, 128.8, 122.8 (dppz); 113.4 ($C_5(CH_3)_5$); 8.9 ($C_5(CH_3)_5$). ^{19}F NMR (H_2O): δ −78.67; IR (KBr, cm^{-1}): ν_{NO} 1846 (vs). UV−vis (H_2O): λ_{max} 286 nm (ϵ = 44 000 cm^{-1} M^{-1}), 360 nm (ϵ = 14 000 cm^{-1} M^{-1}), 380 nm (ϵ = 13000 cm^{-1} M^{-1}). Mp: 260 °C dec. Anal. Calcd for $C_{30}H_{25}F_6N_5O_7RuS_2$ (M_r 846.4): C, 42.55; H, 2.98; N, 8.27; Found: C, 42.42, H, 3.05, N, 8.17.

Aqueous Buffer. All experiments involving DNA were performed in TAE buffer prepared by dissolving 121 g of tris(hydroxymethyl)-aminomethane and 9.3 g of (ethylenedinitrilo)tetraacetic acid, disodium salt, in 500 mL of H_2O. The pH of this solution was adjusted to 8.0 by adding glacial acetic acid. This solution was diluted with H_2O in a 1:50 ratio to produce a solution buffered at pH = 7.7.

Photolysis of 1 and 2. In a typical experiment, 5 mg of **2**[OTf]$_2$ was dissolved in H_2O and placed in an NMR tube. The tube was then photolyzed for 3 h and the spectrum measured again. The characteristic peaks of complex $\mathbf{2}^{2+}$ were still present, and no additional peaks were observed. The tube was then photolyzed for an additional 14 h, a brown precipitate was observed, and only traces of $\mathbf{2}^{2+}$ could be detected. Similar results were obtained upon photolysis of **1[OTf]**$_2$, although 36 h of photolysis were required. For photolysis of **2[OTf]**$_2$ in TAE buffer, a 0.1 mM solution of **2[OTf]**$_2$ was placed in a 1.0 cm polystyrene UV−vis cuvette and photolyzed for 15 min. The UV−vis spectrum was measured, and the process was repeated on the same sample for a total of 90 min of photolysis. Decomposition of $\mathbf{2}^{2+}$ was apparent due to the discoloration of the solution and the broadening and ca. 10% intensity loss of the characteristic peaks at 360 and 380 nm. The cuvette did not transmit wavelengths under 300 nm.

DNA Cleavage by 2[OTf]$_2$. Measurements were performed using 0.8% agarose gels developed in TAE buffer, and the DNA was visualized by rinsing with an ethidium bromide solution. Complex **2[OTf]**$_2$ was dissolved in H_2O or TAE buffer, diluted to 14−40 μM, and allowed to react with DNA plasmid pLCS792 (30 μM nucleotides) for 30 min. Photolysis of reaction mixtures in polypropylene microcentrifuge tubes for 5−30 min resulted in a much less mobile band that indicated DNA cleavage. Photolysis for longer than 30 min caused all DNA bands to disappear. The total volume of a single experiment was 10 μL, and the microcentrifuge tubes did not transmit wavelengths below 290 nm. In experiments with 0.1−0.5 mM H_2O_2 and $K_2S_2O_8$, similar concentrations were used, but the reaction mixtures were heated at 40 °C for 1 h in the dark; some cleavage in these lanes was observed. The addition of DMPO (50 mM) had no effect on the photocleavage reaction with **2**[OTf]$_2$, and DMPO itself displayed no interaction with the plasmid. Cleavage of plasmid pLCS792 by the restriction enzyme *BamH I* and DNase (deoxyribonuclease) was also performed under the same experimental conditions to provide a comparison to the cleavage observed in the presence of compound **2**[OTf]$_2$. In the case of *BamH I*, a single sharp band was observed with a reduced mobility. Treatment of pLCS792 with deoxyribonuclease (DNase) resulted in a band with reduced mobility and another band that correlated to unreacted plasmid. In this case, the band with reduced mobility appeared in the same region as the band observed in the photolysis of **2**[OTf]$_2$ with plasmid.

EPR Studies. To 4-mm quartz EPR tube were added 80 μM solutions of **1[OTf]**$_2$ and **2[OTf]**$_2$ in TAE buffer and H_2O. After the tubes were frozen with liquid N_2 and cooled to 14 K in the spectrometer, no signals were observed. The tubes were then warmed to room temperature and photolyzed for 3 h. Remeasurement of the EPR spectrum at 14 K revealed a broad signal at g = 2.00.

For room temperature spin trapping, 40 μM solutions of **1[OTf]**$_2$ or **2[OTf]**$_2$ in 0.1 M DMPO were used. Both H_2O and TAE buffer were used as solvents. These solutions were placed in polypropylene microcentrifuge tubes and photolyzed for 3.5 h. Aliquots were taken at 0, 30, and 210 min and placed in Pyrex capillaries (1 mm diameter) that were in turn placed in quartz EPR tubes. Initial EPR measurements showed no signals. After 3.5 h, a quartet at g = 2.005 with an A value of 14.9 G was observed for both **1**[OTf]$_2$ and **2**[OTf]$_2$. In both cases an additional signal at g = 2.005 was assigned to a decomposition product of DMPO; it was also observed when DMPO solutions were photolyzed in the absence of metal complexes. Photolysis of **1[OTf]**$_2$ and **2[OTf]**$_2$ in the absence of DMPO did not produce any discernable signals.

Fluorescence Studies. Plasmid pLCS792 was dissolved in TAE buffer and diluted to a 7.4 μM nucleotide concentration. A 2 mL aliquot of this solution was placed in a quartz cuvette and the fluorescence was measured at 600 nm as ethidium bromide (0.25 μM in H_2O) was added. The excitation wavelength was set at 540 nm. The Scatchard equation was used to interpret the data:[27]

$$r/c_f = (n - r)[K_{Etd}/(1 + K_M c_M)]$$

where r is the ratio of bound ethidium to total nucleotides, c_f is the concentration of free ethidium bromide, n is the maximum value of r, K_{Etd} and K_M are the binding constants of ethidium and metal complex, and c_M is the concentration of metal complex. The values of r and c_f were obtained from the fluorescence titration curves and r/c_f vs r is plotted in Figure 7, line 1 for c_M = 0. Additional titrations were performed with increasing concentrations of **2[OTf]**$_2$, giving lines 2−5. Since $K_{obs} = [K_{Etd}/(1 + K_M c_M)]$, plotting $1/K_{obs}$ vs c_M gives a line with a slope of K_M/K_{Etd}. In three successive runs, K_M/K_{Etd} was measured at 4.7, 3.3, and 3.9.

X-ray Diffraction Analyses of 1[OTf]$_2$ and 2[OTf]$_2$. Suitable crystals were mounted vertically on a Siemens P4 autodiffractometer

(27) Howe-Grant, M.; Wu, K. C.; Bauer, W. R.; Lippard, S. J. *Biochemistry* **1976**, *15*, 4339.

and centered optically. In both cases, primitive monoclinic lattices were found for both complexes from the indexing of 25 randomly selected reflections with $15° \leq 2\theta \leq 30°$. Axial photographs confirmed the presence of crystallographic symmetry along the *b* axes. Data collection for **1**$[OTf]_2$ was conducted in the $2\theta-\theta$ mode. The length of the *b* and *c* axes in **2**$[OTf]_2$ led to the selection of ω-scan data collection in this case. Analysis of the systematic absences in data led to the unambiguous selection of the space group $P2_1/c$ for both **1**$[OTf]_2$ and **2**$[OTf]_2$. The data were corrected for absorption by ψ-scan data and the structures were solved using the Patterson routine on the SHELXS-86 program.[28] The structures were refined to anisotropic convergence using the SHELXL-93 full-matrix least-squares process based on F^2.[29]

Acknowledgment. Support from the National Science Foundation (CHE-9215872) to J.L.H. is gratefully acknowledged. We acknowledge the NSF and the Utah State University Research Office for jointly funding the purchase of the USU X-ray (CHE-9002379), EPR (BIR-9413530), and NMR (CHE-9311730) facilities. The authors especially thank Dr. Lance Seefeldt for his generous gift of plasmid and for his consultations. We also thank Drs. Vernon Parker and Greg Swain for assistance with the electrochemical measurements.

Supporting Information Available: Complete listing of X-ray structural data for **1**$[OTf]_2$ and complete listing of X-ray structural data for **2[OTf]**$_2$ (21 pages). Ordering information is given on any current masthead page.

IC950743Z

(28) Sheldrick, G. M. *Acta Crystallogr.* **1990**, *A46*, 467−473.

(29) Sheldrick, G. M. *J. Appl. Crystallogr.*, manuscript in preparation; SHELXL-93 scattering factors from: *International Tables for X-ray Crystallography*; Wilson, A. J. C., Ed.; Kluwer Academic Publishers: Dordrecht, The Netherlands, 1992, Vol. C, Tables 6.1.1.4 (pp 500−502, neutral atom scattering factors), 4.2.6.8 (pp 219−222, f',f''), and 4.2.4.2 (pp 193−199, absorption coefficients). SHELXL-93 is available from Siemens Analytical X-ray Instruments, 6300 Enterprise Lane, Madison, WI 53719, or directly from G. Sheldrick, Institut für Anorganische Chemie der Universität, Tammannstrasse 4, D-37077 Göttingen, Germany: gsheldr@shelx.uni-ac.gwdg.de.